

Small-angle scattering investigations of magnesium hydride used as a hydrogen storage material

Phillip Klaus Pranzas,^{a*} Martin Dornheim,^a Ulrike Bösenberg,^a Jose Ramon Ares Fernandez,^a Guenter Goerigk,^b Stephan Volkher Roth,^c Rainer Gehrke^c and Andreas Schreyer^a

^aInstitut für Werkstofforschung, GKSS Forschungszentrum, Max-Planck-Strasse 1, 21502 Geesthacht, Germany,

^bInstitut für Festkörperforschung, Forschungszentrum Jülich, Postfach 1913, 52425 Jülich, Germany, and

^cHASYLAB, Notkestrasse 85, 22603 Hamburg, Germany. Correspondence e-mail: pranzas@gkss.de

In this work, high-energy ball-milled magnesium hydride samples used for hydrogen storage are investigated using small- and ultra-small-angle neutron scattering (SANS) as well as small-angle X-ray scattering (SAXS). Size distributions of inhomogeneities with dimensions from 10 Å up to more than 10 µm, corresponding to crystallite and particle sizes obtained by X-ray diffraction and electron microscopy, are determined as a function of milling time, milling tool material and added metal oxide catalysts in order to study the influence of the microstructure on the sorption kinetics. Significant changes of the volume fraction distributions are found for samples containing the catalyst chromium oxide, particularly when the catalyst particles are nanometre-sized. Cr₂O₃ is an effective agent for breaking up particles during the milling process. The comparison of SANS and SAXS curves give some of the first information about the distribution of hydrogen-containing structures. Using anomalous small-angle X-ray scattering, an energy-dependent scattering is found for an MgH_x sample with 1 mol% Fe₂O₃. From the separated scattering curve a size distribution of hard spheres is obtained with a size range which is expected for crystallite and particle sizes of the Fe₂O₃ catalyst. Chemical shifts in the absorption spectra give information about the stability of the metal oxide catalysts during the milling process.

© 2007 International Union of Crystallography
Printed in Singapore – all rights reserved

1. Introduction

Metal hydrides are a safe option for hydrogen storage. The metal-hydrogen bond offers the advantage of very high volumetric hydrogen density at a moderate pressure (Reilly & Sandrock, 1980). However, for mobile applications the gravimetric hydrogen density is of importance and light-metal hydrides, based on lithium, aluminium or magnesium, have a high storage capacity by weight. One of the most interesting materials is magnesium hydride, which exhibits a high hydrogen storage capacity of 7.6 wt%. Absorption and desorption kinetics of hydrogen on MgH₂ are well known (Barkhordarian *et al.*, 2003, 2004; Oelerich *et al.*, 2001) as well as cycling and thermal stability (Huhn *et al.*, 2005). The sorption properties are distinctly enhanced by high-energy ball milling and the addition of metal oxide additives, like Fe₂O₃, Nb₂O₅, TiO₂ and Cr₂O₃. The exact function of the additives has not been determined yet. In general, hydrogen absorption on Mg-based lightweight hydrides takes place as a surface reaction consisting of physisorption, dissociation and chemisorption, diffusion into the subsurface and the bulk lattice sites, and hydride formation by nucleation and growth. In the case of desorption, magnesium has to be nucleated and hydrogen atoms have to diffuse to the surface and recombine to hydrogen molecules, which have to desorb physically. The overall hydrogen sorption kinetics of magnesium-based hydrides are determined by the slowest step in this reaction chain. Important factors in improving sorption kinetics are:

- (1) the microstructure of the material, *e.g.* the grain or crystallite size;
- (2) the outer dimension of the material, *e.g.* in case of powdered material, its particle size;
- (3) the use of suitable additives or catalysts.

Besides having a catalytic function, it is known that metal oxide additives influence the milling process and thus the final microstructure and particle size (Dornheim *et al.*, 2006, 2007). One effect is a shift to smaller particle and crystallite sizes during milling. During sorption at higher temperatures the additives prevent rigorous grain growth (Friedrichs *et al.*, 2006). However, structural changes during sorption processes as well as the function and distribution of different additives have hardly been investigated up to now.

In a previous study using small- and ultra-small-angle neutron scattering (SANS/USANS), crystallite and particle sizes of several model MgH_x substances were characterized as a function of hydrogen content and cycling history (Pranzas *et al.*, 2006). The results indicated a crystallite coarsening as well as a break-up of particles of radii larger than 10 µm during the cycling process at a temperature of 573 K. The first SANS/USANS curves of samples with constant hydrogen content using Cr-steel or ceramic (yttrium stabilized ZrO₂ balls and Al₂O₃ vials) milling tools showed apparent differences. Distinct changes in the scattering curves were found in MgH₂ samples using nano- and micro-Cr₂O₃ additives. In the present study, the role of various nano- and micro-metal oxide additives is characterized

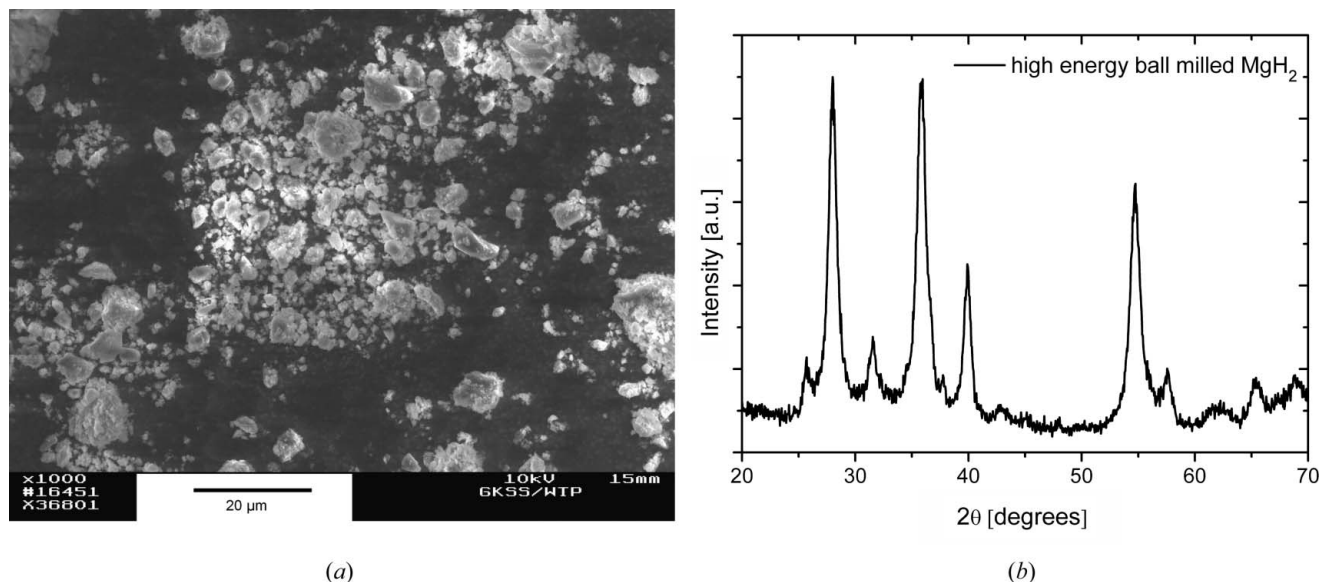


Figure 1
(a) Scanning electron microscopy image of high-energy ball-milled MgH_2 and (b) the X-ray diffraction spectrum of the same sample.

with respect to the influence on the sorption properties using SANS and USANS. Additional small-angle X-ray scattering (SAXS) experiments give information on hydrogen-containing structures and anomalous small-angle X-ray scattering (ASAXS) investigations give information on the distribution and chemical changes of the metal oxide additives.

2. Experimental

The preparation of high-energy ball-milled MgH_x samples in a FritschP5 planetary ball mill with and without addition of metal oxide catalysts was described in Pranzas *et al.* (2006). Hydrogen absorption and desorption was performed at 573 K in a hydrogen titration apparatus. All handling and preparation of the samples was carried out in a continuously purified argon atmosphere.

Scanning electron microscopy (SEM) investigations were performed on a Zeiss DSM 962 instrument. Powder X-ray diffraction (XRD) measurements were carried out on a D8 Bruker ASX using parallel $\text{Cu } K\alpha$ radiation.

SANS measurements were performed at the instrument SANS-2 at the Geesthacht Neutron Facility (GeNF) using distances between the sample and the detector of 1, 3 and 9 m and a wavelength λ of 5.8 Å ($\Delta\lambda/\lambda = 0.1$) as well as a distance of 21 m with $\lambda = 5.8$ and 1.16 Å to cover the q range between 10^{-3} and 0.3 \AA^{-1} , q being the magnitude of the scattering vector defined as $|q| = (4\pi/\lambda) \sin \theta$, 2θ being the scattering angle. Scattering data were normalized by monitor counts and corrected for sample transmission and detector response. The calibration to absolute values was obtained using vanadium. USANS experiments were carried out at the double-crystal diffractometer (DCD) at GeNF (Bellmann *et al.*, 2000) with a wavelength $\lambda = 4.43 \text{ \AA}$, resulting in an accessible q range from 10^{-5} to 10^{-3} \AA^{-1} . For both SANS and USANS investigations, the samples were measured in quartz cuvettes with a thickness of 1 mm. The scattering curves were obtained after desmearing and correction of multiple scattering according to the procedure described in Staron & Bellmann (2002).

Additionally, metal hydride samples were measured at the USAXS beamline BW4 at the Hamburger Synchrotronstrahlungslabor (HASYLAB), using cuvettes with a thickness of 1 mm, a fixed

wavelength of 1.38 Å and distances between the sample and the detector of 2 and 12.6 m.

ASAXS measurements at the B1/JUSIFA (Jülich's user-dedicated small-angle scattering facility, Forschungszentrum Jülich) beamline at HASYLAB were carried out using cuvettes with thicknesses between 0.1 and 1 mm and distances between the sample and the two-dimensional detector of 935 and 3635 mm. The measurements were performed over different energy ranges according to the K -absorption edges of the investigated catalyst metals (*e.g.* Fe: 7112 eV). Up to five energies were used to obtain the energy-dependent scattering. The SAXS curves were corrected for detector sensitivity, empty beam, dark current and transmission. The macroscopic scattering cross section $d\Sigma/d\Omega$ of the ASAXS curves was obtained by calibration with a reference glassy carbon sample.

3. Results and discussion

To characterize the relation between structure and reaction kinetics in the metal hydride systems, microstructural analysis was performed. The first information on the crystallite and particle size distribution was obtained from XRD and SEM investigations. The SEM image in Fig. 1(a) shows MgH_2 without additives after 5 h of high-energy ball milling. From the SEM images a particle size of several micrometres is obtained. In Fig. 1(b) the XRD pattern of the same sample is presented. The crystallite size was obtained from XRD measurements using the Scherrer formula $R = 0.47\lambda/\beta \cos \theta$, where λ is the wavelength, β is the full-width at half-maximum of the peak in radians and θ is the scattering angle. It was found to be around 100 Å.

SEM investigations (not shown) reveal that a formation of agglomerates of the particles takes place during cycling at 573 K. An increasing milling time up to 200 h leads to a further decrease in the crystallite size down to about 50 Å (Aguay-Zinsou *et al.*, 2006).

For a detailed and quantitative analysis of the microstructure, small-angle scattering experiments using neutrons and synchrotron radiation were performed. In Fig. 2(a), combined SANS/USANS curves of three samples are shown, prepared using milling times of 20 and 200 h and using steel and ceramic vials and balls. Differences in the scattering curves are only apparent in the SANS range. The size

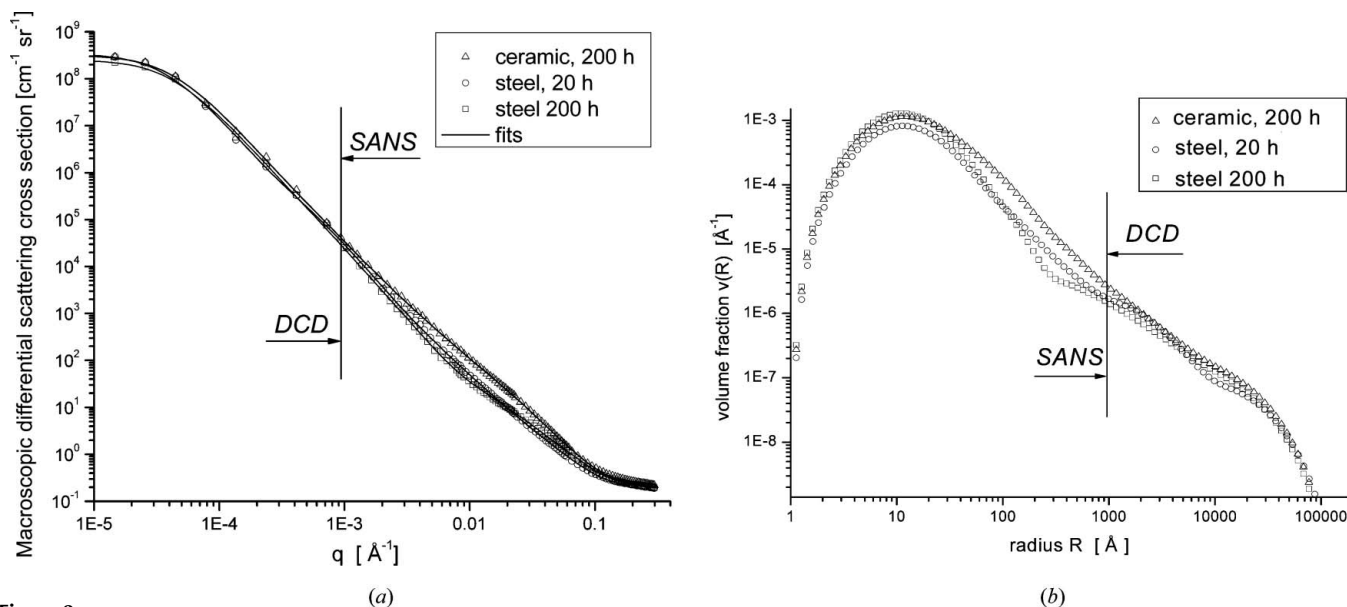


Figure 2

(a) SANS/USANS curves of MgH_2 samples prepared using different milling times as well as different vial and ball materials. The solid lines show the fits obtained during the calculation of the size distributions. (b) Corresponding volume fraction distributions.

distributions were calculated from the SANS/USANS curves using as a first approximation a two-phase model of hard spheres and a constant scattering length density difference $\Delta\eta$ of $3 \times 10^{10} \text{ cm}^{-2}$ between MgH_2 and Mg. The volume fraction distributions obtained are shown in Fig. 2(b).

Particle sizes up to several micrometres and crystallite sizes smaller than 100 \AA are visible in the size distributions, corresponding well to the SEM and XRD results. The maximum of the curves is at a radius of about 20 \AA , which shows that structures with a size of about 40 \AA are obtained in the crystallite range according to this model already after 20 h of high-energy ball milling. The size distributions end at a maximum radius of about 10 \mu m . The curves of the samples prepared with steel vial materials using 20 and 200 h of milling time show small deviations, especially at a radius of about 300 \AA . A larger structural effect is visible comparing the curves prepared by using different vial materials. In the range between a few nanometres and about 1000 \AA the scattering curves are significantly lower for the samples produced

with steel tools. This indicates that the iron in the steel tools supports the decreasing of the crystallite sizes.

A distinct improvement of the sorption kinetics is obtained by the addition of chromium oxide catalyst (Dehouche *et al.*, 2002). In Pranzas *et al.* (2006), SANS/USANS curves of MgH_2 samples after addition of 10 wt% of normal chromium oxide (micro- Cr_2O_3) and commercially available nanoparticles (nano- Cr_2O_3) after 200 h of milling using steel vials and balls were presented with a first interpretation of the scattering curves. Here, the corresponding size distributions shown in Fig. 3 are calculated from the scattering curves using again a two-phase model of hard spheres and a $\Delta\eta$ value of $3 \times 10^{10} \text{ cm}^{-2}$.

The volume fraction distributions of the $\text{MgH}_2/\text{Cr}_2\text{O}_3$ samples look similar to the distributions shown in Fig. 2(b), but have a maximum radius of about 3.5 \mu m , which is apparently smaller than the maximum radii of 10 \mu m or more obtained for other $\text{MgH}_2/M_x\text{O}_y$ systems. Additionally, a distinct lower volume fraction is obtained for the nano- Cr_2O_3 sample in the range of about 400 to $10\,000 \text{ \AA}$ in comparison to the curves of the micro- Cr_2O_3 sample. This shows that the maximum particle size is almost the same using nano- and micro- Cr_2O_3 , whereas the intermediate particle sizes are moved to smaller structures. At a radius of about 300 \AA , the nano- Cr_2O_3 distribution exhibits a broad shoulder, corresponding to a particle size of 750 \AA certified by Sigma-Aldrich for the nano- Cr_2O_3 material (Pranzas *et al.*, 2006).

Additional SAXS investigations were carried out at BW4 at HASYLAB to obtain structural information without the scattering contribution of hydrogen. In Figs. 4(a) and (b) the SANS and SAXS curves of two model MgH_x samples after desorption (' MgH_0 ') and absorption (' MgH_2 ') of hydrogen are compared. The SAXS curves measured in relative intensity units were shifted to the absolute scale of the SANS curves, which are shown after subtraction of the incoherent scattering of hydrogen.

For the sample with a hydrogen content less than 1 wt% (named ' MgH_0 ' in Pranzas *et al.*, 2006) there is only a small difference between the two curves at large q values, mainly originating from the residual hydrogen content. For the sample with a hydrogen content of 7 wt% (' MgH_2 ') the discrepancy clearly increases, starting at a q

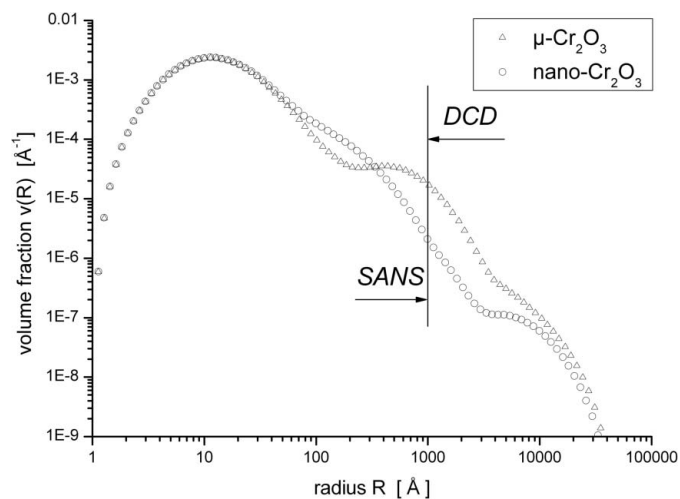


Figure 3

Volume fraction distributions of MgH_2 samples with 10 wt% micro- and nano- Cr_2O_3 additives and 200 h of milling time.

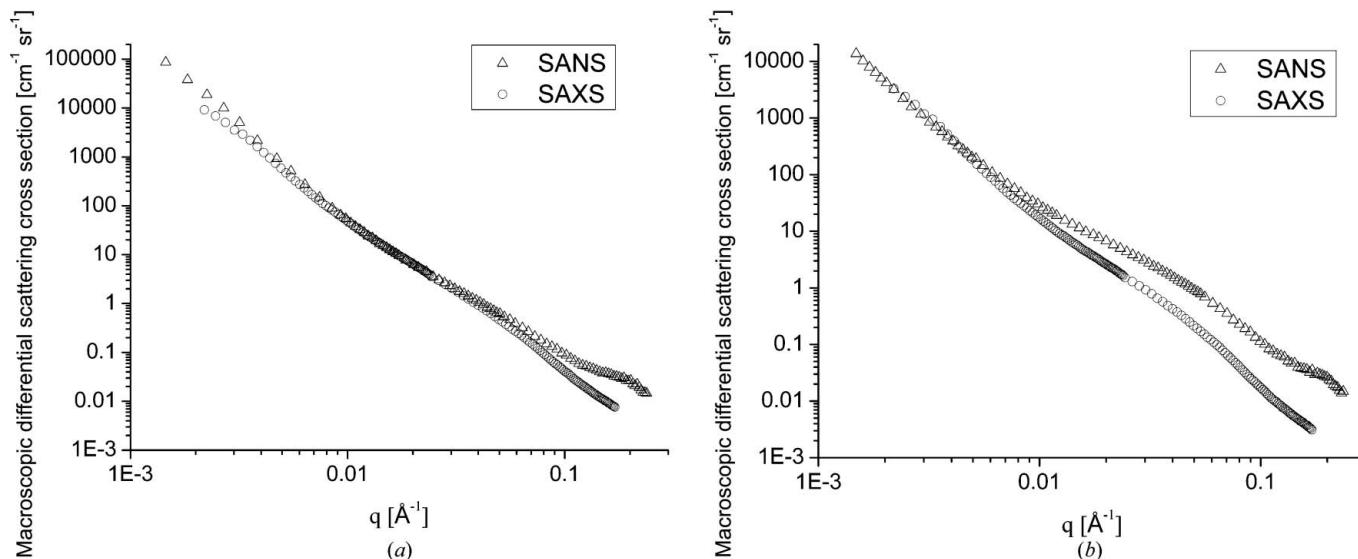


Figure 4 Comparison of SANS and SAXS curves measured at SANS-2 (GeNF) and BW4 (HASYLAB) of MgH_x (a) with desorbed hydrogen (MgH_0) and (b) fully loaded with hydrogen (MgH_2).

value of 0.01 \AA^{-1} , indicating the formation of larger hydrogen-containing structures. A direct subtraction of the SANS and SAXS curves and a further quantitative analysis is not performed because of the different contrast of the two methods. However, a qualitative interpretation is possible. Hydrogenation leads to significant changes in the scattering curves mainly due to an expansion of the Mg lattice and due to changes of the Mg–H/Mg phase boundaries and of the Mg or MgH_2 grain boundaries. Therefore, the difference between the two curves shown in Fig. 4(b) indicates crystallite sizes up to about 600 \AA . Further results from the whole set of SAXS investigations will be published elsewhere.

To obtain information about the distribution of metal oxide catalysts in the MgH_x matrix, anomalous SAXS (ASAXS) measurements were carried out at the B1/JUSIFA beamline at HASYLAB. Besides other catalysts, an energy-dependent scattering was observed, e.g. for

Fe_2O_3 . In Fig. 5 the total scattering curve of $\text{MgH}_{0.9}$ with 1 mol% Fe_2O_3 , measured at 6844 eV, together with the separated scattering after subtraction of the scattering curve measured at 7112 eV, are shown as an example.

As a first estimate neglecting the energy-dependent pore scattering, the size distribution of hard spheres $D(r)$ shown in Fig. 5(b) was calculated from the separated scattering curve using the program *GNOM* (Svergun & Semenyuk, 1991). The two maxima of the distribution with radii of about 100 and 300 \AA are in the size range expected for the crystallite and particle sizes of the Fe_2O_3 catalyst.

Absorption spectra of Fe_2O_3 -containing samples with no chemical shift were measured, which showed the presence of Fe in the sample either from reduced iron oxide during the milling process or from Fe impurities due to the usage of Cr-steel milling tools. Large chemical shifts were found for Nb_2O_5 and TiO_2 , indicating that the catalysts

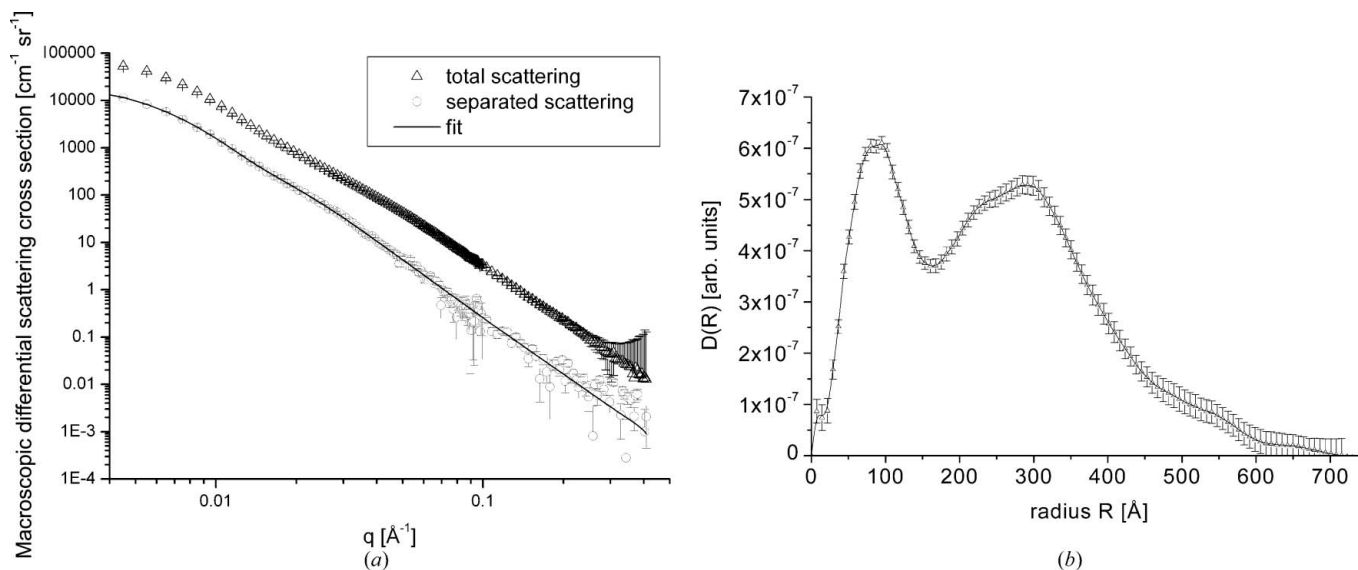


Figure 5 (a) Total scattering curve of $\text{MgH}_{0.9}$ with 1 mol% Fe_2O_3 , measured at 6844 eV, as well as the separated scattering after subtraction of the scattering curve at 7112 eV. (b) Size distribution $D(r)$ of hard spheres calculated from the separated scattering curve (fit: solid line).

remain as metal oxides, even after up to 60 h of milling and several hydrogen sorption cycles.

4. Conclusions

SANS/USANS, SAXS, ASAXS, XRD and SEM investigations were performed to characterize structural changes in MgH_2 systems in order to analyse the relation between structure and reaction kinetics. Particle sizes of several micrometres visible in SEM images and crystallite sizes of about 100 Å or less obtained by XRD measurements were also found in the size distributions calculated from SANS/USANS curves of different MgH_2 samples. The significant influence of milling time, milling-tool material and additives on the microstructure of the hydrides was demonstrated. The addition of Cr_2O_3 leads to a breaking up of particles during the milling process. The maximum particle size obtained by nano- and micro- Cr_2O_3 is almost the same, whereas intermediate particle sizes are moved to smaller structures using nano- Cr_2O_3 . This proves that both chemical composition and initial particle size of the added oxides influence the size distribution and therewith the sorption kinetics.

The first information about the distribution of hydrogen-containing structures was obtained by the comparison of SANS and SAXS curves. Using ASAXS, the size distribution and chemical stability of metal oxide catalysts, particularly Fe_2O_3 , was characterized. This microstructural characterization leads to a better understanding of sorption mechanisms in nanocrystalline light-metal hydrides as well as of the function of the metal oxide catalysts and

gives useful information for the development of these new types of hydrogen storage materials.

References

- Aguey-Zinsou, K.-F., Ares Fernandez, J. R., Klassen, T. & Bormann, R. (2006). *Mater. Res. Bull.* **41**, 1118–1126.
- Barkhordarian, G., Klassen, T. & Bormann, R. (2003). *Scr. Mater.* **49**, 213–217.
- Barkhordarian, G., Klassen, T. & Bormann, R. (2004). *J. Alloys Compd.* **364**, 242–246.
- Bellmann, D., Staron, P. & Becker, P. (2000). *Physica B*, **276**, 124–125.
- Dehouche, Z., Klassen, T., Oelerich, W., Goyette, J., Bose, T. K. & Schulz, R. (2002). *J. Alloys Compd.* **347**, 319–323.
- Dornheim, M., Doppiu, S., Barkhordarian, G., Boesenberg, U., Klassen, T., Gutfleisch, O. & Bormann, R. (2007). *Scr. Mater.* **56**, 841–846.
- Dornheim, M., Eigen, N., Barkhordarian, G., Klassen, T. & Bormann, R. (2006). *Adv. Eng. Mater.* **8**, 377–385.
- Friedrichs, O., Aguey-Zinsou, F., Ares Fernandez, J. R., Sanchez-Lopez, J. C., Justo, A., Klassen, T., Bormann, R. & Fernandez, A. (2006). *Acta Mater.* **54**, 105–110.
- Huhn, P.-A., Dornheim, M., Klassen, T. & Bormann, R. (2005). *J. Alloys Compd.* **404–406**, 499–502.
- Oelerich, W., Klassen, T. & Bormann, R. (2001). *J. Alloys Compd.* **315**, 237–242.
- Pranzas, P. K., Dornheim, M., Bellmann, D., Aguey-Zinsou, K.-F., Klassen, T. & Schreyer, A. (2006). *Physica B*, **385–386**, 630–632.
- Reilly, J. J. & Sandrock, G. D. (1980). *Sci. Am.* **242**, 118–119, 121, 124, 126, 128–129.
- Staron, P. & Bellmann, D. (2002). *J. Appl. Cryst.* **35**, 75–81.
- Svergun, D. I. & Semenyuk, A. V. (1991). *J. Appl. Cryst.* **24**, 537–540.